Research Article

Received: 9 July 2009 Revised: 12 September 2009 Accepted: 14 September 2009 Published online in Wiley Interscience: 16 November 2009

(www.interscience.wiley.com) DOI 10.1002/jctb.2280

Model for a solid-liquid airlift two-phase partitioning bioscrubber for the treatment of BTEX

Jennifer V. Littlejohns, Kim B. McAuley and Andrew J. Daugulis*

Abstract

BACKGROUND: Airlift solid–liquid two-phase partitioning bioreactors (SL-TPPBs) have been shown to be effective for the treatment of gas streams containing benzene, toluene, ethylbenzene and o-xylene (BTEX). The airlift SL-TPPB is a low-energy system that utilizes a sequestering phase of solid silicone rubber beads (10%v/v) that will uptake and release large amounts of BTEX in order to maintain equilibrium conditions within the system. This increases mass transfer from the gas phase during dynamic loading periods and improves degradation performance. This study discusses the development and analysis of a steady-state, tanks-in-series mathematical model, arising from mass balances on BTEX and oxygen in the gas, aqueous and polymer phases to predict the performance of the airlift SL-TPPB over various gas flow rates and BTEX loadings.

RESULTS: An estimability analysis on model parameters determined that the parameters to which model output is most sensitive are those that affect biological activity, which were targeted for estimation. The developed tanks-in-series model was able to predict the removal of BTEX components and dissolved oxygen concentrations over various inlet loadings (20, 60 and 100 mg L^{-1} h^{-1}) and gas flow rates (2,3 and 4 L min^{-1}) that resulted in a range of system performance from effective BTEX treatment to oxygen limiting conditions.

CONCLUSIONS: The model developed, with estimated parameters, provides a valuable tool to determine operating conditions that will result in favourable performance of the airlift SL-TPPB.

Keywords: two-phase partitioning bioreactor; airlift; modelling; BTEX; biodegradation; VOC

NOTATION

A	Cross-sectional area m^2
C	Substrate concentration mg L^{-1}
C^*	Liquid equilibrium concentration mg L^{-1}
D	Diffusion coefficient m^2 s^{-1}
EC	Elimination capacity mg L^{-1} h^{-1}
F_g	Volumetric flow rate L s^{-1}
g	Acceleration due to gravity m^2 s^{-1}
H	Henry's constant
$I_{i2,i}$	Interaction parameter for effect of substrate 2 on initial substrate -
K	Partition coefficient between liquid and polymer mg L^{-1} mg^{-1} L
K_c	Half saturation constant of oxygen mg L^{-1}
K_S	Half saturation constant mg L^{-1}
k_La	Volumetric mass transfer coefficient between gas and liquid s^{-1}
k_l	Liquid side mass transfer coefficient m s^{-1}
k_o	Overall mass transfer coefficient between liquid and polymer m s^{-1}
k_p	Polymer side mass transfer coefficient m s^{-1}
k_d	Endogenous respiration coefficient s^{-1}
M	Molecular weight of the carbon source g mol^{-1}
N	Number of tanks-in-series
Pe	Peclet number
P_G	Power Input W
Q	In a single molecule of carbon source, number of atoms of subscript
Q'	In a single cell, percentage of subscript %
R	Rate of substrate or oxygen depletion mg L^{-1} h^{-1}
R	Radius m
RE	Removal efficiency %
S	Standard deviation
t_c	Circulation time s
T_i^X	Growth substrate transformation capacity = mg_N/mg_G mg mg^{-1}
U	Superficial gas velocity m s^{-1}
$\bar{U}$	Average velocity m s^{-1}
V	Volume L
x_c	Distance traveled by an element of fluid during one circulation m
X	Biomass concentration mg L^{-1}

* *Correspondence to: Andrew J. Daugulis, Department of Chemical Engineering, Queen's University, Kingston, Ontario, K7L 3N6, Canada.*
E-mail: andrew.daugulis@chee.queensu.ca

Department of Chemical Engineering, Queen's University, Kingston, Ontario, K7L 3N6, Canada

$Y_{x/i}$	Yield coefficient for BTEX components mg L^{-1} mg^{-1} L
$Y_{x/O}$	Oxygen growth yeild mg L^{-1} mg^{-1} L

Greek symbols

E	Gas hold-up
μ_{max}	Maximum specific growth rate s^{-1}
Ψ	Proportionality factor
θ	Parameter

Subscripts

b	Bottom section
bio	Biomass
B	Benzene
C	Carbon
d	Downcomer section
d1-d8	Downcomer sections 1 to 8
E	Ethylbenzene
FR#	One of flow rates 2, 3 or 4 L min^{-1}
FR2	Flow rate 2 L min^{-1}
FR3	Flow rate 3 L min^{-1}
FR4	Flow rate 4 L min^{-1}
g	In gas phase
Gl	Between gas and liquid phases
H	Hydrogen
i	Species B,T,E,X or oxygen
In	Inlet gas stream
INH	Inhibitory concentration
l	In liquid phase
Lp	Between liquid and polymer phases
L20	Loading of 20 mg L^{-1} h^{-1}
L60	Loading of 60 mg L^{-1} h^{-1}
L100	Loading of 100 mg L^{-1} h^{-1}
N	Nitrogen
O	Oxygen
p	In polymer phase
R	Riser section
sec	Section of airlift, b, r, t, d1, d2, d3, d4, d5, d6, d7 or d8
t	Top section
T	Toluene
X	o-Xylene

INTRODUCTION

Airlift bioscrubbers provide an energy efficient alternative to stirred tank bioscrubbers for the treatment of volatile organic compound (VOC)-laden gas streams. However, sufficient mass transfer from the gas phase is a concern for both tank configurations due to low solubility of oxygen and potential low solubility of VOCs in water, and oxygen mass transfer of airlift reactors is often slower than in stirred tanks agitated above 400 rpm.[1,2] Recently, Littlejohns and Daugulis[3] investigated an airlift system for the treatment of benzene, toluene, ethylbenzene and o-xylene (BTEX) that contained a second suspended phase of solid silicone rubber beads (10% v/v) with a high affinity for BTEX, called the airlift solid–liquid two-phase partitioning bioreactor (SL-TPPB). The silicone rubber beads served to uptake excess BTEX from the cell containing aqueous phase during increased loading fluctuations which was released back to the aqueous phase according to metabolic demand and maintaining equilibrium conditions. This effectively dampened inlet loading fluctuations by increasing mass transfer from the gas phase, and therefore improved performance, relative to an airlift without a silicone rubber phase. However, it was observed that during operation of the airlift SL-TPPB, oxygen and/or BTEX mass transfer was rate limiting. This prompted investigation of the steady-state performance of the airlift SL-TPPB under various operating conditions (inlet loadings and gas flow rates) in the form of a 3^2 factorial experimental design to identify regions of operating conditions that resulted in increased performance of the system. Using the data provided by the steady-state experimental investigation of the airlift SL-TPPB, the current study describes the development and application of a steady-state mathematical model for the airlift SL-TPPB in order to quantify the observed phenomena and provide a tool to predict performance under various operating conditions.

To model airlift systems, wherein the flow regime lies between the two extremes of perfectly mixed and plug flow[4] causing concentration profiles to vary axially, there are two modeling techniques that are commonly used. The first is the axial dispersion model[5–7] that is based on a one-dimensional Fick's Law type of equation that was developed to describe mixing that slightly deviates from plug flow.[8] The second, more commonly used model, is the tanks-in-series model wherein the number of well-mixed tanks-in-series used to model the system, *N*, describes the level of mixing in the vessel; a higher number of tanks being closer to plug flow and a lower number of tanks in series being closer to well-mixed conditions.[9–11] Tanks-in-series mixing has been shown to provide more accurate predictions in comparison with the axial dispersion model when system hydrodynamics are closer to perfectly well-mixed and is easier to compute numerically[8,12] and was therefore the modeling strategy used in this study. Furthermore, as a well-mixed stirred tank SL-TPPB has previously been modeled for the treatment of BTEX[13], the framework for each tank-in-series and preliminary parameter estimation has been completed.

This study describes the development of a steady-state model for an 11 L airlift SL-TPPB for the treatment of BTEX that was experimentally investigated by Littlejohns and Daugulis.[3] Performance indicators (removal efficiency and elimination capacity) were predicted over various loadings and inlet gas flow rates. An estimability analysis of model parameters was completed in order to identify the parameters to which output is most sensitive. Experimental data were used to assess model accuracy and to estimate the parameters that were most sensitive in order to improve model predictions.

SYSTEM DESCRIPTION

A schematic of the airlift SL-TPPB used by Littlejohns and Daugulis,[3] which is modeled in the current study, can be seen in Fig. 1. In this system, the gas stream containing BTEX is delivered into the vessel below the riser column. The gas bubbles travel up the riser column, transferring BTEX to the liquid phase containing the bacterial consortium. BTEX from the liquid also partitions into the polymer phase. The mixture of the aqueous phase and polymer particles moves downwards in the downcomer column.

AIRLIFT CONCEPTUALIZATION

Previous hydrodynamic characterization of the airlift SL-TPPB using a residence time distribution analysis determined the Peclet numbers (*Pe*) over a range of inlet gas flow rates, which were used to determine the number of tanks-in-series, *N*, from the following

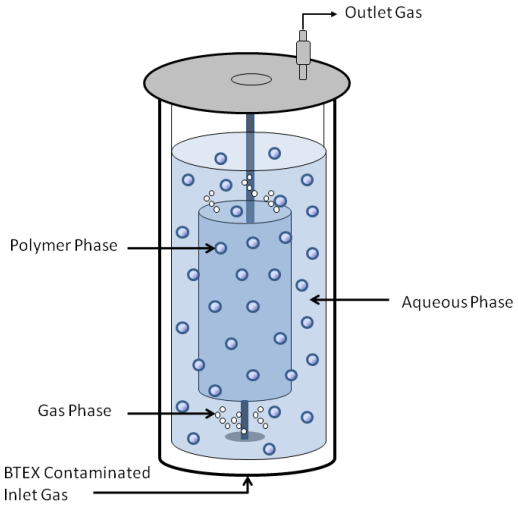

Figure 1. Schematic of the 11 L airlift two-phase partitioning bioscrubber containing silicone rubber polymers (10% v/v) and BTEX degrading bacterial consortium.

correlation:[4,11]

$$N = \frac{Pe}{2} \quad (1)$$

This correlation provides an estimate of the number of tanks-in-series that represent mixing with an inlet flow rate of 2, 3 and 4 L min^{-1} to be 9, 11 and 11, respectively. However, it is known that the downcomer section in airlift systems is nearly plug flow relative to the riser, and has been represented as 10 tanks-in-series by other authors in studies of airlifts of similar size to that used in the current study.[9,11] It has been stated that the number of tanks in series does not have a strong effect on simulation results,[10] and therefore, the number of tanks-in-series used to represent all flow rates was selected to be 11. These 11 well-mixed tanks were distributed as shown in Fig. 2: one as the bottom, one as the riser, one as the top and the remaining eight to represent plug flow in the downcomer section.

MODEL DEVELOPMENT

The model for the airlift SL-TPPB was developed using the following key assumptions:

1. Mixing within the airlift in each phase can be described using the tanks-in-series model.
2. BTEX is transferred from the gas phase to the aqueous phase, and from the aqueous phase to the polymer phase.[14] Direct transfer between the gas-phase and the polymer is neglected.
3. The biomass is distributed throughout the liquid, is constant throughout the reactor and consumes BTEX only from the aqueous phase.
4. All polymer beads are spherical and are the same size.
5. Diffusion coefficients of BTEX in the polymer are constant.
6. Constant partition coefficients describe equilibrium between the liquid and polymer phases. Henry's law describes equilibrium between the gas and liquid phases.
7. Substrate toxicity can be described using the model by Luong.[15]
8. Substrate interactions can be described using the model by Littlejohns and Daugulis.[16]

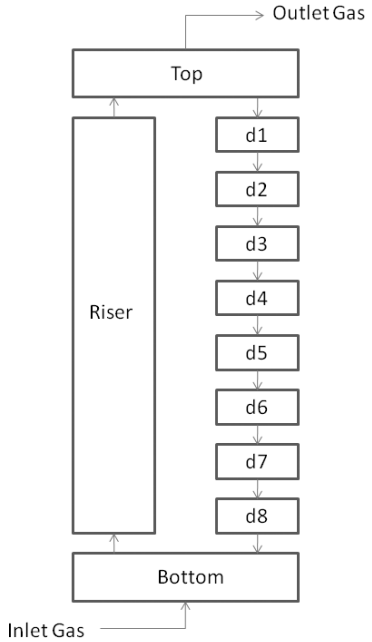

Figure 2. Representation of the 11 L SL-TPPB using tanks-in-series to describe mixing for model development.

9. The specific growth rate has a dependence on oxygen concentrations according to the model described in Bailey and Ollis.[17]
10. A lumped overall mass-transfer coefficient can describe mass transfer from the liquid to the polymer phases.
11. The resistance to mass transfer in the gas phase and microbial cell walls is negligible.
12. Mass transfer of BTEX to/from the headspace to/from the liquid is negligible.
13. Temperature and pH are constant.
14. Polymers have the same circulation velocity as the liquid phase.
15. Polymers do not affect gas-hold up in the reactor.
16. Liquid flow rate is constant in each section of the airlift.

Table 1 lists the steady-state equations developed from mass balances that are used to describe the concentrations of BTEX components and oxygen in the gas (Equations (2)–(6)), aqueous (Equations (7)–(11)) and polymer (Equations (12)–(16)) phases in each CSTR within the airlift SL-TPPB. Biomass concentrations were treated as a model input in order to simplify the system. Although aqueous phase and polymer phase equations were developed to complete the set of equations, these were not used in the objective function or to estimate parameters, as aqueous and polymer phase concentrations were not measured experimentally.

Table 2 contains thermodynamic and kinetic expressions that were substituted into the primary equations listed in Table 1. The thermodynamic expressions that are used to determine concentrations in the aqueous phase in equilibrium with the gas phase and the polymer phase are listed as Equations (17) and (18), respectively, in Table 2. Kinetic expressions that were developed previously[16] were combined with models to account for substrate toxicity[15] and oxygen limitations,[17] and are shown in Table 2 as Equations (19), (20), (21) and (22) for benzene, toluene, ethylbenzene and o-xylene, respectively. In addition, an expression for oxygen consumption by biomass is shown

Table 1. List of equations for airlift SL-TPPB Model

Gas-phase balances		
Bottom section	$F_{g,in}\frac{C_{i,in}}{V_{b,g}} + F_{g,d}\frac{C_{i,d8,g}}{V_{b,g}} - k_L a_i\left(C^*_{i,in,gl} - C_{i,b,l}\right)\frac{V_{b,l}}{V_{b,g}} - k_L a_i\left(C^*_{i,d8,gl} - C_{i,b,l}\right)\frac{V_{b,l}}{V_{b,g}} - F_{g,r}\frac{C_{i,b,g}}{V_{b,g}} = 0$	2
Top section	$F_{g,r}\frac{C_{i,r,g}}{V_{t,g}} - k_L a_i\left(C^*_{i,r,gl} - C_{i,t,l}\right)\frac{V_{t,l}}{V_{t,g}} - F_{g,d}\frac{C_{i,t,g}}{V_{t,g}} - \left(F_{g,r} - F_{g,d}\right)\frac{C_{i,t,g}}{V_{t,g}} = 0$	3
Riser section	$F_{g,r}\frac{C_{i,b,g}}{V_{r,g}} - k_L a_i\left(C^*_{i,b,gl} - C_{i,r,l}\right)\frac{V_{r,l}}{V_{r,g}} - F_{g,r}\frac{C_{i,r,g}}{V_{r,g}} = 0$	4
Downcomer section #1	$F_{g,d}\frac{C_{i,t,g}}{V_{d1,g}} - k_L a_i\left(C^*_{i,t,gl} - C_{i,d1,l}\right)\frac{V_{d1,l}}{V_{d1,g}} - F_{g,d}\frac{C_{i,d1,g}}{V_{d1,g}} = 0$	5
Downcomer section z Z = 2 to 8	$F_{g,d}\frac{C_{i,d_{Z-1},g}}{V_{d1,g}} - k_L a_i\left(C^*_{i,dz-1,gl} - C_{i,dz,l}\right)\frac{V_{d1,l}}{V_{d1,g}} - F_{g,d}\frac{C_{i,d_Z,g}}{V_{d1,g}} = 0$	6
Liquid-phase balances		
Bottom section	$k_L a_i\left(C^*_{i,in,gl} - C_{i,b,l}\right) + k_L a_i\left(C^*_{i,d8,gl} - C_{i,b,l}\right) + F_l\frac{C_{i,d8,l}}{V_{b,l}} - F_l\frac{C_{i,b,l}}{V_{b,l}} - \frac{3k_{O,i}}{R_p}\left(C_{i,b,l} - C^*_{i,b,lp}\right) - r_i = 0$	7
Top section	$F_l\frac{C_{i,r,l}}{V_{t,l}} - F_l\frac{C_{i,t,l}}{V_{t,l}} + k_L a_i\left(C^*_{i,r,gl} - C_{i,t,l}\right)\frac{1}{V_{t,l}} - \frac{3k_{O,i}}{R_p}\left(C_{i,t,l} - C^*_{i,t,lp}\right) - r_i = 0$	8
Riser section	$F_l\frac{C_{i,b,l}}{V_{r,l}} - F_l\frac{C_{i,r,l}}{V_{r,l}} + k_L a_i\left(C^*_{i,b,gl} - C_{i,r,l}\right) - \frac{3k_{O,i}}{R_p}\left(C_{i,r,l} - C^*_{i,r,lp}\right) - r_i = 0$	9
Downcomer section #1	$F_l\frac{C_{i,t,l}}{V_{d1,l}} - F_l\frac{C_{i,d1,l}}{V_{d1,l}} + k_L a_i\left(C^*_{i,t,gl} - C_{i,d1,l}\right) - \frac{3k_{O,i}}{R_p}\left(C_{i,d1,l} - C^*_{i,d1,lp}\right) - r_i = 0$	10
Downcomer section z Z = 2 to 8	$F_l\frac{C_{i,dz-1,l}}{V_{d1,l}} - F_l\frac{C_{i,dz,l}}{V_{d1,l}} + k_L a_i\left(C^*_{i,dz-1,gl} - C_{i,dz,l}\right) - \frac{3k_{O,i}}{R_p}\left(C_{i,dz,l} - C^*_{i,dz,lp}\right) - r_i = 0$	11
Polymer-phase balances		
Bottom section	$F_p\frac{C_{i,d8,p}}{V_{b,p}} - F_p\frac{C_{i,b,p}}{V_{b,p}} + \frac{3k_{O,i}}{R_p}\left(C_{i,b,l} - C^*_{i,b,lp}\right)\frac{V_{b,l}}{V_{b,p}} = 0$	12
Top section	$F_p\frac{C_{i,r,p}}{V_{t,p}} - F_p\frac{C_{i,t,p}}{V_{t,p}} + \frac{3k_{O,i}}{R_p}\left(C_{i,t,l} - C^*_{i,t,lp}\right)\frac{V_{t,l}}{V_{t,p}} = 0$	13
Riser section	$F_p\frac{C_{i,b,p}}{V_{r,p}} - F_p\frac{C_{i,r,p}}{V_{r,p}} + \frac{3k_{O,i}}{R_p}\left(C_{i,r,l} - C^*_{i,r,lp}\right)\frac{V_{r,l}}{V_{r,p}} = 0$	14
Downcomer section #1	$F_p\frac{C_{i,t,p}}{V_{d1,p}} - F_p\frac{C_{i,d1,p}}{V_{d1,p}} + \frac{3k_{O,i}}{R_p}\left(C_{i,d1,l} - C^*_{i,d1,lp}\right)\frac{V_{d1,l}}{V_{d1,p}} = 0$	15
Downcomer section Z Z = 2 to 8	$F_p\frac{C_{i,d_{z-1},p}}{V_{d_1,p}} - F_p\frac{C_{i,d_Z,p}}{V_{d_1,p}} + \frac{3k_{O,i}}{R_p}\left(C_{i,dz,l} - C^*_{i,dz,lp}\right)\frac{V_{d_1,l}}{V_{d_1,p}} = 0$	16

as Equation (23). Performance indicators, which are the focus of this study, include elimination capacity (Equation (24)) and removal efficiency (Equation (25)) and are shown in Table 2, which are functions of the predicted BTEX concentrations in the outlet gas, and were the outputs modeled in this work.

PARAMETER VALUES AND MODEL INPUTS

Parameters values and model inputs were obtained directly from literature values and from empirical correlations that utilize literature values and/or physical dimensions of the system components. Those parameter values and model inputs that were obtained from correlations will be described in more detail below. A list of all parameter values and their origin can be seen in Table 3, and a list of all model input values, all of which were a function of gas flow rate, can be seen in Table 4.

Correlations for parameter values

The correlations used in this study to determine parameter values utilized estimates from the literature and/or dimensions of system components, and allowed for the determination of volumetric mass transfer coefficients for BTEX over various inlet gas flow rates ($k_L a_{B,FR\#}$, $k_L a_{T,FR\#}$, $k_L a_{E,FR\#}$, $k_L a_{X,FR\#}$), the overall mass transfer coefficient for oxygen, $k_{o,O}$ and the oxygen growth yield, $Y_{X/O}$.

Volumetric mass transfer coefficients for BTEX over various inlet gas flow rates, $k_L a_{B,FR\#}$, $k_L a_{T,FR\#}$, $k_L a_{E,FR\#}$, $k_L a_{X,FR\#}$

Volumetric mass transfer coefficients are a function of inlet gas flow rate, which is an operating condition that is varied in this study. Therefore, volumetric mass transfer coefficients for BTEX were determined for each flow rate used. To determine volumetric mass transfer coefficients for BTEX in the airlift reactor, volumetric mass transfer coefficients for oxygen over flow rates of 2, 3 and 4 L min^{-1} previously determined by Littlejohns and Daugulis[2] in an airlift SL-TPPB were utilized in Equation (26).[22]

$$k_L a_{i,FR\#} = \psi \cdot k_L a_{O,FR\#} \tag{26}$$

The parameter ψ was estimated using Equation (27).[22]

$$\psi = D_i \Big/ D_O \tag{27}$$

Diffusion coefficients used in Equation (27) for oxygen and BTEX in water at 30 °C are 3.51×10^{-5}, 1.17×10^{-5}, 1.03×10^{-5}, 9.33×10^{-6} and 9.33×10^{-6} $cm^2\ s^{-1}$, respectively.[24]

Overall oxygen mass transfer coefficient, $k_{o,O}$

The overall mass transfer coefficient for BTEX between aqueous and polymer phases must consider both aqueous and polymer resistances to mass transfer. The overall mass transfer coefficient

Table 2. Thermodynamic and kinetic expressions

Equilibrium expressions

$$C^*_{i,\mathrm{sec},gl} = C_{i,\mathrm{sec},g} \Big/ H_{\mathrm{lg}} \quad (17)$$

$$C^*_{i,\mathrm{sec},lp} = C_{i,\mathrm{sec},p} \Big/ K_{lp} \quad (18)$$

Kinetic expressions

$$r_{B,\mathrm{sec}} = \frac{\dfrac{\mu_{\max,B} C_{B,\mathrm{secc},l}}{(K_{s,B} + C_{B,\mathrm{sec},l}) + I_{T,B} C_{T,\mathrm{sec},l} + I_{X,B} C_{X,\mathrm{sec},l}} \left(1 - \dfrac{C_{B,\mathrm{sec},l}}{C_{B,INH}}\right) X_{\mathrm{sec}}}{Y_{X/B}} \left(\frac{C_{O,\mathrm{sec},l}}{K_{c,B} + C_{O,\mathrm{sec},l}}\right) \quad (19)$$

$$r_{T,\mathrm{sec}} = \frac{\dfrac{\mu_{\max,T} C_{T,\mathrm{sec},l}}{(K_{s,T} + C_{T,\mathrm{sec},l}) + I_{B,T} C_{T,\mathrm{sec},l}} \left(1 - \dfrac{C_{T,\mathrm{sec},l}}{C_{T,INH}}\right) X_{\mathrm{sec}}}{Y_{X/T}} \left(\frac{C_{O,\mathrm{sec},l}}{K_{c,T} + C_{O,\mathrm{sec},l}}\right) \quad (20)$$

$$r_{E,\mathrm{sec}} = \frac{\dfrac{\mu_{\max,E} C_{E,\mathrm{sec},l}}{(K_{s,E} + C_{E,\mathrm{sec},l})} \left(1 - \dfrac{C_{E,\mathrm{sec},l}}{C_{E,INH}}\right) X_{\mathrm{sec}}}{Y_{X/E}} \left(\frac{C_{O,\mathrm{sec},l}}{K_{c,E} + C_{O,\mathrm{sec},l}}\right) \quad (21)$$

$$r_{X,\mathrm{sec}} = \left(T^X_B \left(\frac{dC_{B,\mathrm{sec},l}}{dt}\left(\frac{1}{X_{\mathrm{sec}}}\right)\right)\right)\left(\frac{C_{X,\mathrm{sec},l}}{K_{s,X} + C_{X,\mathrm{sec},l}}\right) X_{\mathrm{sec}} + \left(T^X_T \left(\frac{dC_{T,\mathrm{sec},l}}{dt}\left(\frac{1}{X_{\mathrm{sec}}}\right)\right)\right)\left(\frac{C_{X,\mathrm{sec},l}}{K_{s,X} + C_{X,\mathrm{sec},l}}\right) X_{\mathrm{sec}} \quad (22)$$

$$r_{O,\mathrm{sec}} = \left(r_{B,\mathrm{sec}} Y_{X/B} + r_{T,\mathrm{sec}} Y_{X/T} + r_{E,\mathrm{sec}} Y_{X/E}\right) \Big/ Y_{X/O} \quad (23)$$

Key performance indicators

$$EC = \frac{F_g(C_{i,in} - C_{i,t,g})}{V_{total}} \quad (24)$$

$$RE = \frac{(C_{i,in} - C_{i,t,g})}{C_{i,in}} \times 100\% \quad (25)$$

was calculated using Equation (28).[25]

$$\frac{1}{k_{O,i}} = \frac{1}{K_i k_{p,i}} + \frac{1}{k_{l,i}} \quad (28)$$

In order to determine mass transfer coefficients on the liquid and polymer sides, semi-empirical equations can be used which are shown as Equation (29)[25] and Equation (30), respectively.[26]

$$k_{l,i} = \frac{D_{O,l}}{R_p} \quad (29)$$

$$k_{p,i} = \frac{D_{O,p}\pi^2}{2R_p} \quad (30)$$

The diffusivity of oxygen in silicone rubber is 3.4×10^{-5} cm^2 s^{-1}.[27]

Oxygen growth yield, $Y_{X/O}$

The oxygen growth yield can be estimated using the correlation developed by Mateles,[28] shown as Equation (31).

$$Y_{X/O} = \left[16\left(\frac{2Q_C + Q_H/2 - Q_O}{Y_{X/i} \cdot M} + \frac{Q'_O}{1600} - \frac{Q'_C}{600} + \frac{Q'_N}{933} - \frac{Q'_H}{200}\right)\right]^{-1} \quad (31)$$

The composition of the bacterial consortium used in this study, which is composed of bacteria of the genus *Pseudomonas*, was approximated using the composition of *Escherichia coli*, as they are both gram negative rods.[29] The composition of *Escherichia coli* is typically reported as 50 wt% carbon, 8 wt% hydrogen, 20 wt% oxygen and 14 wt% nitrogen.[30,31] $Y_{X/O}$ was approximated for the BTEX mixture by using the average of Equation (31) for each BTEX component.

Correlations and equations for model inputs

The correlations and equations used in this study to determine model inputs, which are functions of inlet flow rate, utilized literature values and dimensions of system components, and allowed for the determination of gas, liquid and polymer volumes in each section ($V_{g,sec,FR\#}$, $V_{l,sec,FR\#}$, $V_{p,sec,FR\#}$), gas flow rates ($F_{g,d,FR\#}$, $F_{g,r,FR\#}$), and liquid and polymer flow rates ($F_{l,FR\#}$, $F_{p,FR\#}$).

Volumes of gas, liquid and polymer in each airlift section, $V_{g,sec,FR\#}$, $V_{l,sec,FR\#}$, $V_{p,sec,FR\#}$

The gas volumes in the riser, downcomer, top and bottom sections in the airlift SL-TPPB are a function of inlet gas flow rate and can be approximated using Equations (32), (33), (34) and (35), respectively, under the assumption that $\varepsilon_r = \varepsilon_t = \varepsilon_b$.[11]

$$V_{g,r,FR\#} = V_r \varepsilon_{r,FR\#} \quad (32)$$

$$V_{g,d,FR\#} = V_d \varepsilon_{d,FR\#} \quad (33)$$

$$V_{g,t,FR\#} = V_t \varepsilon_{r,FR\#} \quad (34)$$

$$V_{g,b,FR\#} = V_b \varepsilon_{r,FR\#} \quad (35)$$

Gas hold-up in the airlift was estimated using Equation (36),[32] which can be used to determine the hold-up in the riser and dowcomer sections in Equation (37) and Equation (38),[32] respectively.

$$\varepsilon_{FR\#} = 4.334 \times 10^{-3} \left(\frac{P_g}{V_l}\right)^{0.499}_{FR\#} \quad (36)$$

$$\varepsilon_{FR\#} = 0.89 \varepsilon_{r,FR\#} \quad (37)$$

$$\varepsilon_{FR\#} = \frac{A_r \varepsilon_{r,FR\#} + A_d \varepsilon_{d,FR\#}}{A_r + A_d} \quad (38)$$

A preliminary estimate of the energy requirements for the airlift for use in Equation 36 can be made using Equation (39).[32]

$$\left(\frac{P_g}{V_l}\right)_{FR\#} = \frac{\rho_l g U_{g,r,FR\#}}{1 + \dfrac{A_d}{A_r}} \quad (39)$$

where $U_{g,r}$ was found to be 0.0042, 0.0064 and 0.0085 m s^{-1} for inlet flow rates of 2, 3 and 4 L min^{-1}.

The volumes of liquid and polymer in each section were then determined by subtracting the volume of gas in a section from the total volume of the section; the remaining volume consisted of 10% polymers and 90% aqueous phase. The total volume for the top section was determined by subtracting the aqueous volume of the other airlift sections from the total liquid volume of 11 L, and then accounting for 10% polymers and the gas hold-up in the top section.

Table 3. Initial parameter values

Parameter	Value: Flow 2 L min^{-1}	Value: Flow 3 L min^{-1}	Value: Flow 4 L min^{-1}	Unit	S_θ	Method of Estimation
$k_L a_B$	0.00069	0.001	0.0013	s^{-1}	0.0026	Current study
$k_L a_T$	0.00061	0.00089	0.0012	s^{-1}	0.0023	Current study
$k_L a_E$	0.00057	0.00083	0.0011	s^{-1}	0.0022	Current study
$k_L a_X$	0.00057	0.00083	0.0011	s^{-1}	0.0022	Current study
$k_L a_O$	0.002	0.003	0.004	s^{-1}	0.0005	Littlejohns and Daugulis[2]
K_B	62			mg L^{-1} solid L mg^{-1} aqueous	2.88	Littlejohns and Daugulis[18]
K_T	200			mg L^{-1} solid L mg^{-1} aqueous	19.5	Littlejohns and Daugulis[18]
K_E	414			mg L^{-1} solid L mg^{-1} aqueous	153.08	Littlejohns and Daugulis[18]
K_X	593			mg L^{-1} solid L mg^{-1} aqueous	86.4	Littlejohns and Daugulis[18]
K_O	10			mg L^{-1} solid L mg^{-1} aqueous	2	Shiku *et al.*[19]
H_B	0.26			mg L^{-1} gas L mg^{-1} aqueous	0.04	Littlejohns and Daugulis[18]
H_T	0.35			mg L^{-1} gas L mg^{-1} aqueous	0.02	Littlejohns and Daugulis[18]
H_E	0.43			mg L^{-1} gas L mg^{-1} aqueous	0.02	Littlejohns and Daugulis[18]
H_X	0.25			mg L^{-1} gas L mg^{-1} aqueous	0.03	Littlejohns and Daugulis[18]
H_O	34.17			mg L^{-1} gas L mg^{-1} aqueous	2	Sandler (http://www.henrys-law.org)[20]
$K_{o,B}$	1.05×10^{-8}			m s^{-1}	1.84×10^{-6}	Littlejohns *et al.*,[13]
$K_{o,T}$	9.3×10^{-9}			m s^{-1}	1.63×10^{-6}	Littlejohns *et al.*,[13]
$K_{o,E}$	8.5×10^{-9}			m s^{-1}	1.48×10^{-6}	Littlejohns *et al.*,[13]
$K_{o,X}$	1.04×10^{-7}			m s^{-1}	1.48×10^{-6}	Littlejohns *et al.*,[13]
$K_{o,O}$	3.06×10^{-8}			m s^{-1}	3.06×10^{-6}	Shown in current study
$\mu_{max,B}$	0.00012			s^{-1}	0.0018	Littlejohns and Daugulis[16]
$\mu_{max,T}$	0.00017			s^{-1}	0.0023	Littlejohns and Daugulis[16]
$\mu_{max,E}$	0.000036			s^{-1}	0.006	Littlejohns and Daugulis[16]
$K_{s,B}$	27.57			mg L^{-1}	11.01	Littlejohns and Daugulis[16]
$K_{s,T}$	34.12			mg L^{-1}	12.12	Littlejohns and Daugulis[15]
$K_{s,E}$	0.36			mg L^{-1}	1.76	Littlejohns and Daugulis[16]
$K_{s,X}$	0.1			mg L^{-1}	10	Littlejohns and Daugulis[16]
$I_{T,B}$	2			–	0.5	Littlejohns and Daugulis[16]
$I_{X,B}$	−0.7			–	0.5	Littlejohns and Daugulis[16]
$I_{B,T}$	−0.4			–	0.5	Littlejohns and Daugulis[16]
$I_{E.B}$	4			–	0.5	Littlejohns and Daugulis[16]
$C_{B,INH}$	20			mg L^{-1}	15	Abuhamed *et al.*[21]
$C_{T,INH}$	20			mg L^{-1}	15	Abuhamed *et al.*[21]
$C_{E,INH}$	35			mg L^{-1}	15	Estimated from Abuhamed *et al.*[21]
$C_{X,INH}$	35			mg L^{-1}	15	Estimated from Abuhamed *et al.*[21]
$Y_{X/B}$	1.35			mg mg^{-1}	0.27	Littlejohns and Daugulis[16]
$Y_{X/T}$	1.25			mg mg^{-1}	0.25	Littlejohns and Daugulis[16]
$Y_{X/E}$	0.85			mg mg^{-1}	0.17	Littlejohns and Daugulis[16]
$Y_{X/O}$	0.94			mg mg^{-1}	0.2	Shown in current study
$T_B X$	0.5			–	0.1	Littlejohns and Daugulis[16]
$T_T X$	0.5			–	0.1	Littlejohns and Daugulis[16]
k_d	2.5×10^{-6}			s^{-1}	1×10^{-7}	Littlejohns *et al.*,[13]
$K_{C,B}$	0.5			mg L^{-1}	0.2	Bailey and Ollis[17]
$K_{C,T}$	0.5			mg L^{-1}	0.2	Bailey and Ollis[17]
$K_{C,X}$	0.5			mg L^{-1}	0.2	Bailey and Ollis[17]

Table 4. Input values

Input	Value: Flow 2 L min^{-1}	Value: Flow 3 L min^{-1}	Value: Flow 4 L min^{-1}	Unit	Method of estimation
$C_{in,i,L20}$	0.46	0.31	0.23	mg L^{-1}	Measured
$C_{in,i,L60}$	1.37	0.92	0.69	mg L^{-1}	Measured

Table 4. (*Continued*)

Input	Value			Unit	Method of estimation
	Flow 2 L min^{-1}	Flow 3 L min^{-1}	Flow 4 L min^{-1}		
$C_{in,i,L100}$	2.29	1.52	1.15	mg L^{-1}	Measured
$C_{in,Bio,L20}$	1140	1420	1800	mg L^{-1}	Measured
$C_{in,Bio,L60}$	1500	1920	2400	mg L^{-1}	Measured
$C_{in,Bio,L100}$	1600	2960	2670	mg L^{-1}	Measured
F_l	0.368	0.482	0.535	L s^{-1}	Current Study
F_p	0.042	0.055	0.061	Ls^{-1}	Current Study
$F_{g,in}$	0.0333	0.05	0.0667	L s^{-1}	Measured
$F_{g,r}$	0.04	0.061	0.081	L s^{-1}	Current Study
$F_{g,d}$	0.0071	0.011	0.015	L s^{-1}	Current Study
$V_{l,b}$	0.573	0.571	0.569	L	Current Study
$V_{l,t}$	1.84	1.88	1.91	L	Current Study
$V_{l,r}$	3.67	3.65	3.64	L	Current Study
$V_{p,d}$	0.0544	0.0542	0.054	L	Current Study
$V_{g,b}$	0.0129	0.0158	0.0183	L	Current Study
$V_{g,t}$	0.0417	0.0425	0.0432	L	Current Study
$V_{g,r}$	0.08	0.10	0.12	L	Current Study
$V_{g,d}$	0.0098	0.012	0.014	L	Current Study

Gas flow in riser and downcomer, $F_{g,d,FR\#}$, $F_{g,r,FR\#}$

The gas flow rate in the downcomer and riser were determined for the inlet gas flow rates used in this study using Equation (40) and (41), respectively.

$$F_{g,d,FR\#} = \varepsilon_{d,FR\#} A_d \overline{U}_{l,FR\#} \quad (40)$$

$$F_{g,r,FR\#} = F_{in,FR\#} + F_{g,d,FR\#} \quad (41)$$

In order to evaluate $F_{g,d,FR\#}$ from Equation (40), $\bar{U}_l$ must also be determined for various inlet air flow rates, which can be estimated using Equation (42).[32]

$$\overline{U}_{l,FR\#} = \frac{x_c}{t_{c,FR\#}} \quad (42)$$

In order to determine the circulation time, $t_{c,FR\#}$, the data obtained from the tracer experiment for various inlet air flow rates described in Littlejohns and Daugulis[2] were used.

Liquid and polymer flow rates, $F_{L,FR\#}$, $F_{P,FR\#}$

The liquid and polymer flow rate in the airlift SL-TPPB can be calculated using Equation (43) and (44), respectively, over various flow rates.

$$F_{l,FR\#} = \overline{U}_{FR\#} A_r \left(1 - \varepsilon_{r,FR\#}\right)(1 - 0.1) \quad (43)$$

$$F_{p,FR\#} = \overline{U}_{l,FR\#} A_r (0.1) \quad (44)$$

MODELING

Solid-Liquid TPPB data

The experimental data modeled in this study were obtained from Littlejohns and Daugulis[3], which consisted of nine runs at various operating conditions in an airlift SL-TPPB. A continuous gas stream containing BTEX was delivered into the system, and measurements were obtained until steady-state biomass concentrations were reached (>200 h). Various operating conditions were tested using a 3^2 factorial design at inlet loadings of 20, 60 and 100 mg L^{-1} h^{-1} and inlet gas flow rates of 2, 3 and 4 L min^{-1}. During these runs, inlet and outlet gas-phase concentrations of BTEX components and DO concentrations were measured. Rotameter settings fluctuated considerably, causing fluctuations in inlet and outlet BTEX concentrations during experimental runs. Average performance indicators were reported and used to estimate model parameters and assess model accuracy.

Numerical methods

Matlab™ was used to generate model predictions by solving the non-linear set of equations shown in Table 1 for each BTEX component and oxygen using the solver fsolve. As stated previously, inlet concentrations fluctuated during experimental operation due to minor increases or decreases in the rotameter settings. Therefore, individual BTEX inlet gas phase concentrations were approximated by taking the average measured inlet total BTEX concentrations and assuming each component was delivered into the system in equal amounts, as these proportions remained relatively constant throughout experimentation. The inlet BTEX gas-phase concentrations, along with experimentally measured biomass concentrations, which were used as a model input, are listed in Table 4.

Parameter estimates, as described in the following section, were determined by finding the parameter values that minimize the objective function, which was a weighted sum of squared errors between the model predictions and the experimental performance indicators for BTEX components and DO concentrations. The 'lsqnonlin' Matlab™ routine was used to obtain the parameter estimates.

Estimability analysis and parameter estimation

The estimability analysis and parameter estimation were completed using methods similar to those used for a stirred-tank SL-TPPB model by Littlejohns *et al.*[13] An estimability analysis of the 55 parameters in the model was completed to determine which parameters had the largest impact on model predictions, while taking

into account correlated effects of parameters and uncertainty in initial parameter values. This estimability analysis was followed by estimation of the most important parameters, within realistic upper and lower bounds, to obtain improved parameter values that fit the SL-TPPB data better than the initial parameter values listed in Table 3. The estimability analysis ranked the parameters according to their influence on model outputs, correlation with other model parameters and uncertainty in initial values using the method described by Kou *et al*.[33] The parametric sensitivity coefficients were scaled appropriately using uncertainties in the initial parameter values and in the measured responses.[34] The uncertainty scaling factors S_θ for the initial parameter guesses are shown in Table 3.

The parameters that were ranked highest using the estimability analysis are those that are most estimable, because these parameters have the greatest influence on model predictions and have little correlation with the effects of other parameters with higher rank. The high ranking parameters were, therefore, the targets for estimation using experimental data from the nine steady-state airlift SL-TPPB runs. The model predictions were fitted to the experimental data by minimizing an objective function consisting of the sum of squared errors weighted by uncertainties in measured BTEX performance indicators (RE and EC) and DO concentrations. The standard deviations used as weighting factors in the objective function and during estimability analysis were 1.3% for RE, 0.7 mg L^{-1} h^{-1} for EC and 0.5% for DO, respectively. Upper and lower bounds (see Table 5) on the estimated parameters were used to ensure that the estimated values remained physically realistic. A series of parameter-estimation calculations was performed, beginning with the most estimable parameter ($\mu_{max,E}$, by itself) followed by the two most estimable parameters ($\mu_{max,E}$ *and* $K_{s,X}$) then the three and so on. Parameter estimation stopped when including additional parameters did not cause a noticeable decrease in the objective function for parameter estimation.

Table 5. Ranking and parameter estimates

Estimability rank	Parameter	Upper/Lower bounds	Estimated value
1	$\mu_{max,E}$	0.00057/0.000017	0.00011
2	$K_{S,X}$	1.5/0.001	0.54
3	$\mu_{max,T}$	0.0026/0.000086	0.00053
4	$\mu_{max,B}$	0.0022/0.000092	0.00062
5	$I_{E,B}$	1/−1	0.0014
6	$I_{X,B}$	1/−1	−0.0056
7	$k_La_{E,FR2}$	0.0097/0.00087	0.0019
8	$k_La_{B,FR2}$	0.0056/0.00066	0.00082
9	$k_La_{O,FR3}$	0.0051/0.00041	0.00083
10	$k_La_{O,FR2}$	0.0051/0.00041	0.00087
11	$k_La_{O,FR3}$	0.0071/0.00071	0.001
12	$k_La_{E,FR3}$	0.0081/0.00091	0.0031
13	$k_La_{B,FR3}$	0.0095/0.00085	0.0016
14	$k_La_{T,FR2}$	0.0009/0.0001	0.0006
15	$k_La_{T,FR3}$	0.0072/0.00092	0.0022
16	$k_La_{B,FR4}$	0.0079/0.00082	0.0019
17	$k_La_{T,FR4}$	0.0071/0.0009	0.0021
18	$I_{T,B}$	3/−3	2
19	$I_{B,T}$	2.2/−2.4	−0.4
20	$Y_{X/O}$	1.04/0.34	.93
21	$k_La_{X,FR2}$	0.0027/0.00017	.00056
22	$k_La_{E,FR4}$	0.011/0.0011	0.005
23	$k_{o,B}$	$8.8 \times 10^{-7}/8.8 \times 10^{-9}$	9.1×10^{-8}
24	$k_La_{X,FR3}$	0.0033/0.00013	0.00083
25	$K_{S,E}$	7.12/0.0002	2.12
26	$k_{o,X}$	—	—
27	$Y_{X/B}$	—	—

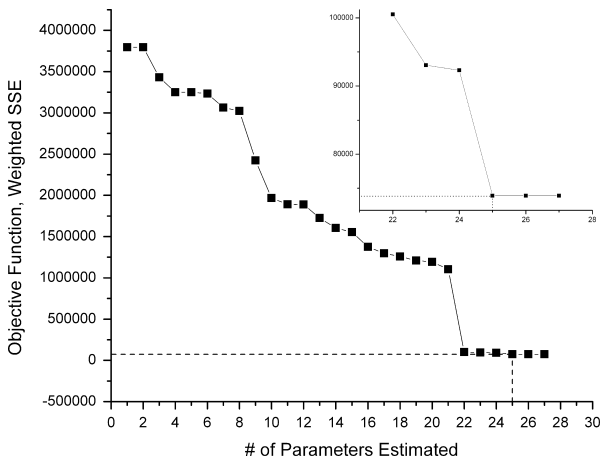

Figure 3. Objective function with increasing number of estimated parameters. Dotted line represents the plateau in objective function and the corresponding number of estimated parameters. Inset displays objective function over limited range to display plateau at 25 estimated parameters.

RESULTS AND DISCUSSION

Estimability analysis and parameter estimation

The estimability analysis and parameter estimation were completed to identify and estimate parameters to improve model predictions. The ranked list of parameters (from most estimable to least estimable) is shown in Table 5. Using the experimental data for RE and EC for each BTEX component and oxygen concentrations from the nine runs completed in the airlift SL-TPPB, the estimability analysis permitted the ranking of over 27 parameters. It is, therefore, confirmed that the amount of data collected will allow for the estimation of at least 27 parameters. The parameters that ranked the highest were those that govern the rate of biological degradation. These ranking results are similar to those found for the model for the stirred-tank SL-TPPB on which the stirred tank model structure in this current study was based.[13] Other parameters that were ranked highly are gas–liquid volumetric mass-transfer coefficients for BTEX and oxygen, particularly at an inlet gas flow rate of 2 L min^{-1}. This high ranking can be attributed to the fact that the experimental data indicate that the system was oxygen limited at an inlet gas flow rate of 2 L min^{-1}. In addition, the system is sensitive to volumetric mass-transfer coefficients because, if the rate of gas–liquid mass transfer is not rapid, mass transfer will limit the rates of biodegradation and uptake by polymers.

The appropriate number of parameters to estimate in this model was evaluated by increasing the number of parameters estimated, in the order of their rank listed in Table 5, and determining when the objective function no longer reduced appreciably. A plot of the objective function for parameter estimation, as a function of the number of parameters estimated, is shown in Fig. 3. This figure indi-

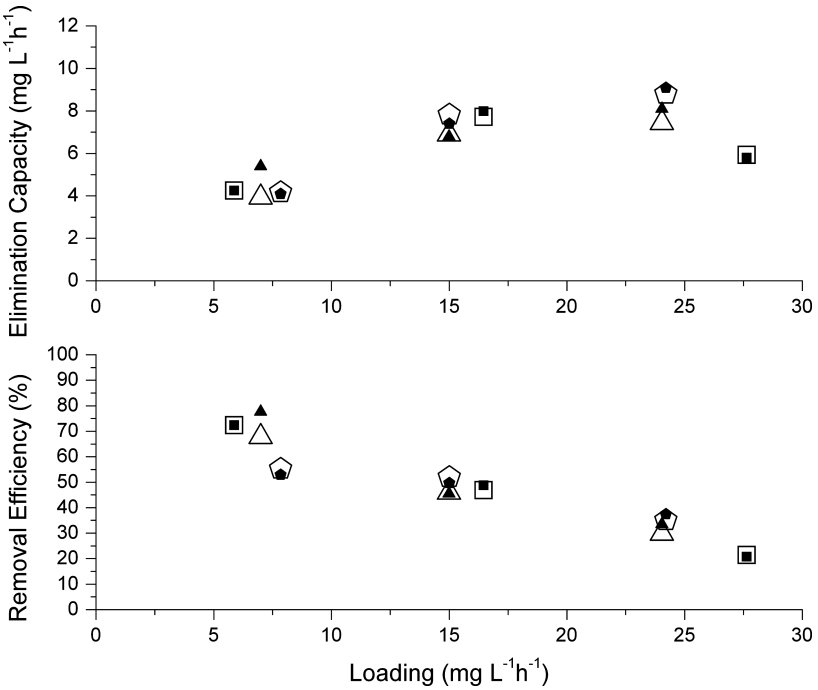

Figure 4. Removal efficiencies and elimination capacities for benzene during steady-state operation over a range of loadings. Inlet gas flow rates of 2 L min^{-1} (squares), 3 L min^{-1} (triangles), and 4 L min^{-1} (pentagons) are shown for experimental data (solid) and model predictions (hollow).

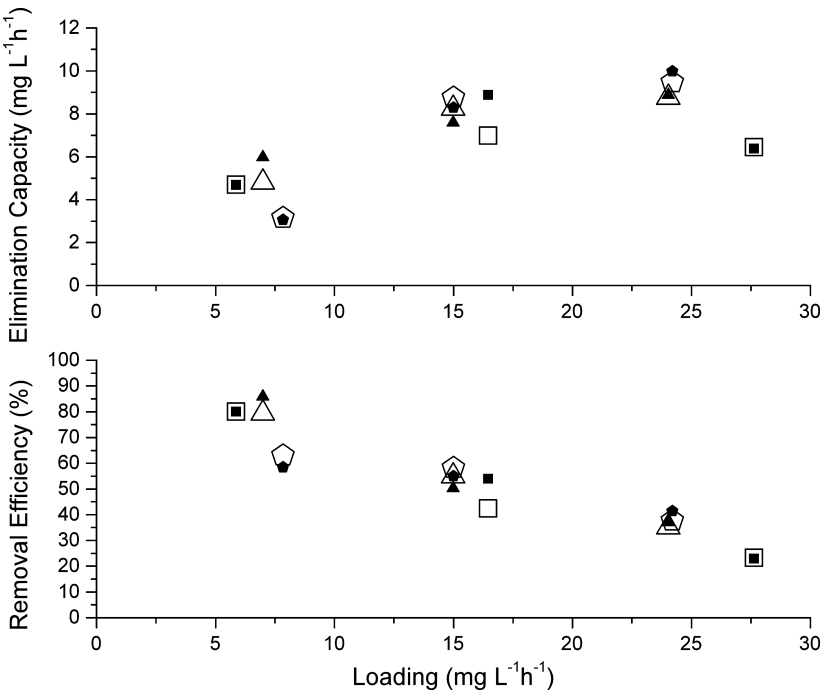

Figure 5. Removal efficiencies and elimination capacities for toluene during steady-state operation over a range of loadings. Inlet gas flow rates of 2 L min^{-1} (squares), 3 L min^{-1} (triangles), and 4 L min^{-1} (pentagons) are shown for experimental data (solid) and model predictions (hollow).

cates that little improvement to the model fit can be obtained by estimating more than 25 parameters. Estimates for the 25 top-ranked parameters are shown in Table 5. The remaining 30 parameters were held at their initial values because these parameters had little influence on the model predictions or were already well-known (small uncertainties, S_θ). One interesting observation is that specific growth rates were predicted to be an order of magnitude faster than the initial parameter values, which were estimated by Littlejohns *et al.*[13] to fit to experimental stirred-tank SL-TPPB. This may be due to the fact that the airlift SL-TPPB is gas–liquid mass transfer limited, whereas the smaller stirred-tank SL-TPPB was kinetically limited. Furthermore, in the current study the oxygen volumetric

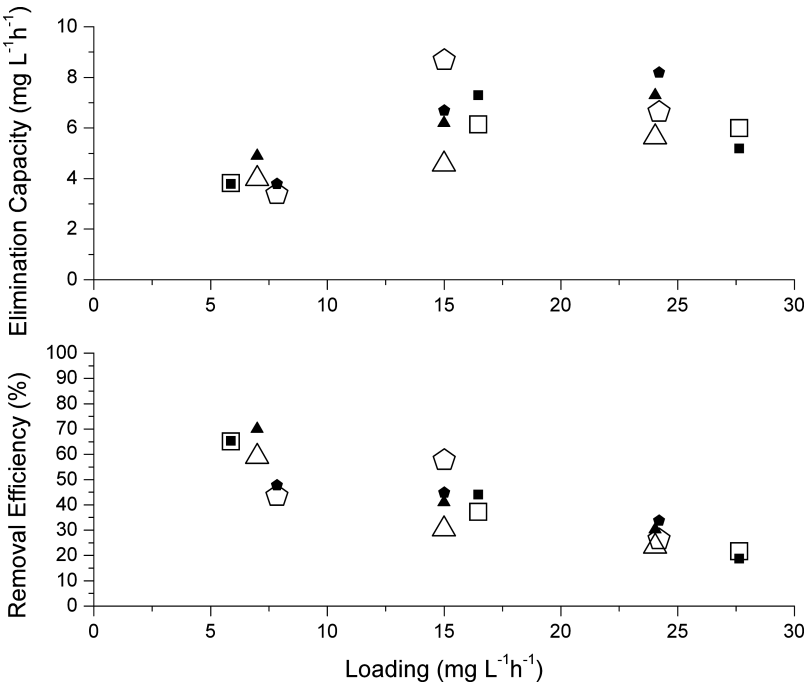

Figure 6. Removal efficiencies and elimination capacities for ethylbenzene during steady-state operation over a range of loadings. Inlet gas flow rates of 2 L min^{-1} (squares), 3 L min^{-1} (triangles), and 4 L min^{-1} (pentagons) are shown for experimental data (solid) and model predictions (hollow).

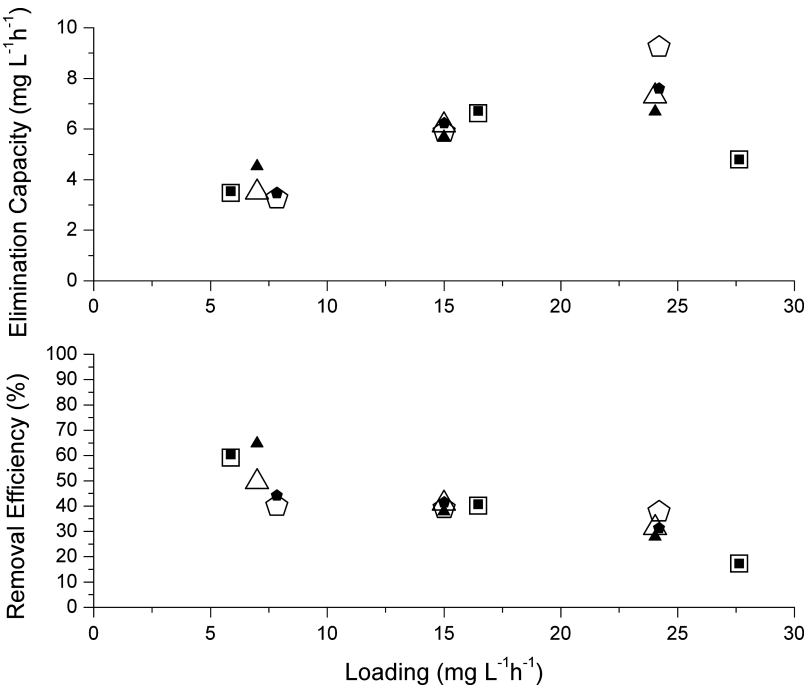

Figure 7. Removal efficiencies and elimination capacities for o-xylene during steady-state operation over a range of loadings. Inlet gas flow rates of 2 L min^{-1} (squares), 3 L min^{-1} (triangles), and 4 L min^{-1} (pentagons) are shown for experimental data (solid) and model predictions (hollow).

mass-transfer coefficients were consistently estimated to be significantly lower than their initial values. The mass-transfer coefficients estimated in the current study indicate that oxygen mass-transfer limitations influence the performance of the SL-TPPB.

It should be noted that the values of the growth rates for benzene and toluene are larger than previously reported in literature, but are of the same order of magnitude as those reported by Reardon *et al.*[35] which were 0.73 and 0.86 h^{-1}, respectively. However, as the objective of this study is to show the applicability of the model to fit to the experimental data, and not to obtain true parameter values, the estimated growth rate values were deemed acceptable.

Model predictions

Predictions of the performance indicators are plotted, along with experimental data, for benzene, toluene, ethylbenzene and

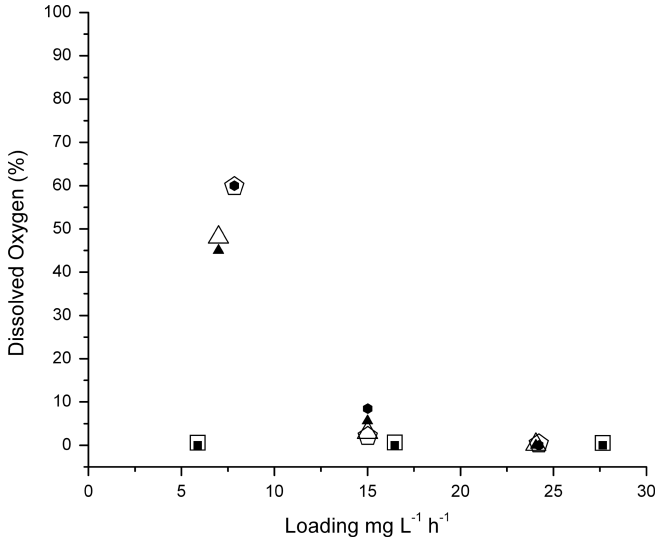

Figure 8. Dissolved oxygen concentrations during steady-state operation over a range of loadings. Inlet gas flow rates of 2 L min^{-1} (squares), 3 L min^{-1} (triangles), and 4 L min^{-1} (pentagons) are shown for experimental data (solid) and model predictions (hollow).

o-xylene in Figs 4, 5, 6 and 7, respectively. It can be seen that the predicted performance indicators fit the experiment data quite well, particularly at an inlet gas flow rate of 2 L min^{-1} and the lowest loading of 20 mg L^{-1} h^{-1} total BTEX (approximately 5 mg L^{-1} h^{-1} each component). The predictions for ethylbenzene RE and EC at a loading of 60 mg L^{-1} h^{-1} total BTEX (approximately 15 mg L^{-1} h^{-1} ethylbenzene) appear to deviate the most from the experimental data, however, only by approximately 15%. The results show that the model can predict the trend of decreasing REs with increasing loadings for all compounds. The model predictions at a loading of 20 mg L^{-1} h^{-1} total BTEX (approximately 5 mg L^{-1} h^{-1} each component) and an inlet gas flow rate of 3 L min^{-1} are consistently lower than the experimental performance indicators (e.g. by 13% for xylene RE). The model predicts that these are the best operating conditions (from the nine different runs) as the performance indicators are the highest at these conditions. Note that the performance at the lower loading of 20 mg L^{-1} h^{-1} total BTEX (approximately 5 mg L^{-1} h^{-1} each component) and 2 L min^{-1} is predicted to have similar performance.

Figure 8 shows the predicted and experimental DO concentrations for each set of operating conditions. The model has the capability to predict that the system is oxygen limited at the inlet gas flow rate of 2 L min^{-1} for all loadings, which is reflected in the ECs in Figs 4–7. In these figures, values for both the predictions and experimental data plateau at a total BTEX loading of 60 mg L^{-1} h^{-1} (approximately 15 mg L^{-1} h^{-1} each component). The model also successfully predicts that at the flow rates of 3 and 4 L min^{-1} and a loading of 20 mg L^{-1} h^{-1} (approximately 5 mg L^{-1} h^{-1} each component), there is ample DO within the system, which is an important system characteristic for enabling effective BTEX removal.

The predicted concentration profile in each section of the airlift shown in Fig. 2, for each BTEX compound, can be seen in Fig. 9 for a loading of 20 mg L^{-1} h^{-1} total BTEX (approximately 5 mg L^{-1} h^{-1} each component) and an inlet gas flow rate of 3 L min^{-1}. It can be seen that the concentrations of benzene, toluene and ethylbenzene in the gas phase decrease significantly in the bottom, riser and top stages of the airlift and subsequently plateau in the downcomer sections. Note that the decrease in gas-phase xylene concentrations in the bottom, riser and top sections is less pronounced. The fraction (in each section) of the total amount of each compound degraded is represented by the size of the bubbles in Fig. 9. The fraction degraded is largest in the riser section for benzene, toluene and ethylbenzene, but is largest in the bottom section for xylene. A total of 57, 75 and 59% of the benzene, toluene and ethylbenzene, respectively, is removed in the bottom, riser and top sections. However, only 32% of the

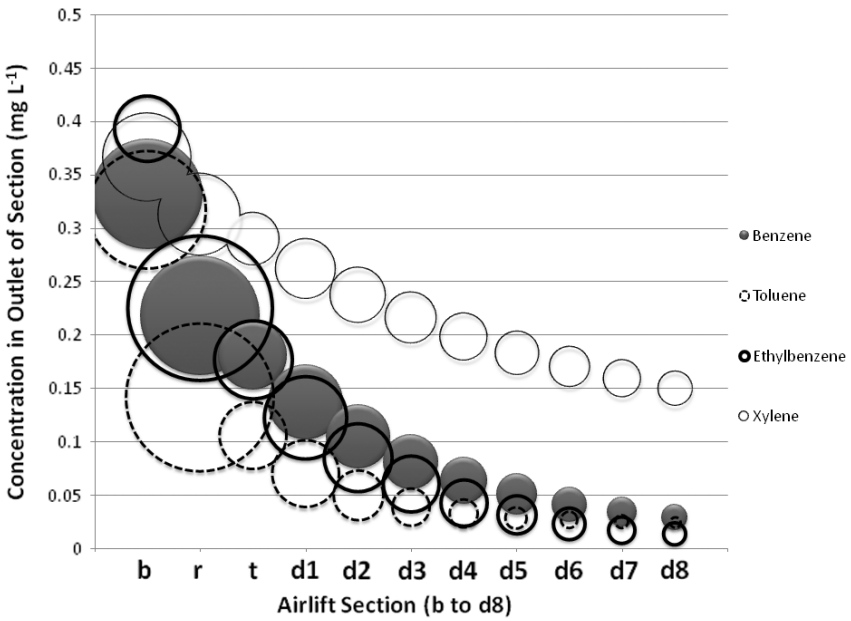

Figure 9. Predicted gas phase concentration distribution in airlift for a gas flow rate of 3 L min^{-1} and a loading rate of 20 mg L^{-1} h^{-1}. Center of bubble corresponding to y-axis represents the concentration in the outlet of airlift section, size of bubble corresponds to percentage fraction of total compound degraded in airlift section.

xylene is removed in these three initial stages. Toluene and xylene, in particular, have very distinct removal profiles in the airlift which may be due to the volumetric mass-transfer coefficients for xylene being lower than those for toluene at a flow rate of 3 L min^{-1} (by 38%), causing the removal from the gas phase to be initially much more rapid for toluene in comparison to xylene.

CONCLUSIONS

A steady-state tanks-in-series model has been developed to model removal efficiency, elimination capacity and dissolved oxygen concentrations in an airlift SL-TPPB for the treatment of gas streams containing BTEX. An estimability analysis on model parameters revealed that the microbial kinetic parameters have the greatest influence on model predictions. Experimental data from the operation of the airlift SL-TPPB at steady-state over a range of loadings and inlet gas flow rates was used to estimate parameters and assess model accuracy. BTEX volumetric mass-transfer coefficients were estimated to be smaller in comparison with values obtained for a stirred-tank SL-TPPB, indicating that mass-transfer limitations are more important in the airlift system than in the smaller well-mixed system. The model is capable of predicting performance indicators and dissolved oxygen concentrations in the airlift SL-TPPB over a range of loadings (20 to 100 mg L^{-1} h^{-1}) and inlet gas flow rates (2 to 4 L min^{-1}). In addition, the model predicts that the riser section removes the largest fraction of BTEX within the airlift and that a smaller fraction is removed in the downcomer sections.

ACKNOWLEDGEMENTS

The financial support of the Natural Sciences and Engineering Research Council of Canada is gratefully acknowledged.

REFERENCES

1 Fontana RC, Polidoro TA and da Silveira MM, Comparison of stirred tank and airlift bioreactors in the production of polygalacturonases by *Aspergillus oryzae*. *Bioresource Technol* **100**:4493–4498 (2009).
2 Littlejohns JV and Daugulis AJ, Oxygen mass transfer and hydrodynamics in a multi–phase bioscrubber system. *Chem Eng Sci* **64**:4171–4177 (2009).
3 Littlejohns JV and Daugulis AJ, A Two–Phase Partitioning Airlift Bioreactor for the Treatment of BTEX Contaminated Gases. *Biotechnol Bioeng* **103**:1077–1086 (2009).
4 Swaine DE and Daugulis AJ, Review of liquid mixing in packed bed biological reactors. *Biotechnol Prog* **4**:134–148 (1988).
5 Nikakhtari H and Hill GA, Continuous bioremediation of phenol-polluted air in an external loop airlift bioreactor with a packed bed. *J Chem Technol Biotechnol* **81**:1029–1038 (2006).
6 Sikula I and Markoš J, Modeling of enzymatic reaction in an airlift reactor using an axial dispersion model. *Chem Papers* **62**:10–17 (2008).
7 Jia X, Wen J, Jiang Y, Liu X and Feng W, Modeling of batch phenol biodegradation in internal loop airlift bioreactor with gas recirculation by Candida tropicalis. *Chem Eng Sci* **61**:3463–3475 (2006).
8 Turner JR and Mills PL, Comparison of axial dispersion and mixing cell models for design and simulation of Fischer-Tropsch slurry bubble column reactors. *Chem Eng Sci* **45**:2317–2324 (1990).
9 Kanai T, Ichikawa J, Yoshikawa H and Kawase Y, Dynamic modeling and simulation of continuous airlift bioreactors. *Bioprocess Eng* **23**:213–220 (2000).
10 Sikula I, Juraščík M and Markoš J, Modelling of enzymatic reaction in an internal loop airlift reactor. *Chem Papers* **60**:446–453 (2006).
11 Znad H, Bales V and Kawase Y, Modeling and scale up of airlift bioreactor. *Comput Chem Eng* **28**:2765–2777 (2004).
12 Abu-Reesh IM and Abu-Sharkh BF, Comparison of axial dispersion and tanks–in–series models for simulating the performance of enzyme reactors. *Ind Eng Chem Res* **42**:5495–5505 (2003).
13 Littlejohns JV, McAuley KB and Daugulis A, Model for a Solid-Liquid Stirred Tank Two-Phase Partitioning Bloscrubber for the Treatment of BTEX. *J Hazard Mater* DOI:10.1016/j.j hazmat.2009.10.091.
14 Kars RL, Best RJ and Drinkenburg AAH, The sorption of propane in slurries of active carbon in water. *Chem Eng J* **17**:201–210 (1997).
15 Luong JHT, Generalization of monod kinetics for analysis of growth data with substrate inhibition. *Biotechnol Bioeng* **29**:242–248 (1987).
16 Littlejohns JV and Daugulis AJ, Kinetics and interactions of BTEX compounds during degradation by a bacterial consortium. *Process Biochem* **43**:1068–1076 (2008).
17 Bailey J and Ollis D, *Biochemical Engineering Fundamentals*, 2nd edn. McGraw Hill Book Company, New York (1986).
18 Littlejohns JV and Daugulis AJ, Response of a solid–liquid two-phase partitioning biroeactor to transient BTEX loadings. *Chemosphere* **73**:1453–1460 (2009).
19 Shiku H, Saito T, Wu C–C, Yasukawa T, Yokoo M, Abe H, *et al*, Oxygen permeability of surface modified poly(dimethysiloxane) characterized by scanning electrochemical microscopy. *Chem Lett* **35**:234–235 (2006).
20 Sandler R, Compilation of Henry's Law Constants for Inorganic and Organic Species of Potential. Importance in Environmental Chemistry (Version 3). Available: http://www.henrys–law.org, (2009).
21 Abuhamed T, Bayraktar E, Mehmetoglu T and Mehmetoglu Ü, Kinetics model for growth of *Pseudomonas putida* F1 during benzene, toluene and phenol biodegradation. *Process Biochem* **39**:983–988 (2004).
22 Metcalf and Eddy Inc., *Wastewater Engineering: Treatment, Disposal, Reuse*. McGraw-Hill, New York (1991).
23 Nielsen J and Villadsen J, *Bioreaction Engineering Principles*. Plenum Publishing, New York (1994).
24 EPA (U.S. Environmental Protection Agency), Diffusion Coefficient Estimation – Extended Input Range (2006).
25 Ma JW, Cunningham MF, McAuley KB, Keoshkerian B and Georges MK, Interfacial mass transfer in nitroxide-mediated miniemulsion polymerization. *Macromol Theory Simul* **11**:953–960 (2002).
26 Yao KZ, McAuley KB and Marchildon EK, Simulation of continuous solid-phase polymerization of nylon 6,6. III. Simplified model. *J Appl Polym Sci* **89**:3701–3712 (2003).
27 Merkel TC, Bondar VI, Nagai K, Freeman BD and Pinnau I, Gas sorption, diffusion, and permeation in poly(dimethylsiloxane). *J Polym Sci Part B: Polym Phys* **38**:415–434 (2000).
28 Mateles RI, Calculation of the oxygen requriment for cell production. *Biotechnol Bioeng* **13**:581–582 (1971).
29 Buchanan RE and Gibbons NE, *Bergey's Manual of Determinative Bacteriology*. Waverly Press Inc., Baltimore (1974).
30 Nicholson W, Department of Veterinary Science and Microbiology, Microbiology Physiology Course, University of Arizona. Available: http://www.microvet.arizona.edu/Courses/MIC328/mic328index.html, (2005).
31 Todar K, Microbiology Webbed Out Online textbook. Available: http://www.bact.wisc.edu/Microtextbook, (2000).
32 Chisti MY, *Airlift Bioreactors*. Elsevier, Essex (1989).
33 Kuo J, *Practical Design Calculations for Groundwater and Soil Remediation*. Lewis Publishers, New York (1999).
34 Thompson DE, McAuley KB and McLellan PJ, Parameter estimation in a simplified MWD model for HDPE produced by a Ziegler–Natta catalyst. *Macromol React Eng* **3**:160–177 (2009).
35 Reardon KF, Mosteller DC and Rogers JB, Biodegradation kinetics of benzene, toluene, and phenol as single and mixed substrates for *Pseudomonas putida* F1. *Biotechnol Bioeng* **69**:385–400 (2000).

